INTERNATIONAL JOURNAL FOR NUMERICAL METHODS IN ENGINEERING
Int. J. Numer. Meth. Engng 2010; **83**:1700–1718
Published online 15 June 2010 in Wiley Online Library (wileyonlinelibrary.com). DOI: 10.1002/nme.2878

Multi-time-step domain coupling method with energy control

N. Mahjoubi[1] and S. Krenk[2,*,†]

[1]*Université de Lyon, INSA-Lyon, LaMCoS, CNRS UMR5259, F-69621 Villeurbanne, France*
[2]*Department of Mechanical Engineering, Technical University of Denmark, DK-2800 Lyngby, Denmark*

SUMMARY

A multi-time-step integration method is proposed for solving structural dynamics problems on multiple domains. The method generalizes earlier state-space integration algorithms by introducing displacement constraints via Lagrange multipliers, representing the time-integrated constraint forces over the individual time step. It is demonstrated that displacement continuity between the subdomains leads to cancelation of the interface contributions to the energy balance equation, and thus stability and algorithmic damping properties of the original algorithms are retained. The various subdomains can be integrated in time using different time steps and/or different state-space time integration schemes. The solution of the constrained system equations is obtained using a dual Schur formulation, allowing for maximum independence of the calculation of the subdomains. Stability and accuracy are illustrated by a numerical example using a refined mesh around concentrated forces. Copyright © 2010 John Wiley & Sons, Ltd.

Received 25 August 2009; Revised 24 January 2010; Accepted 25 January 2010

KEY WORDS: state-space time integration; multi-time-step method; dual Schur domain decomposition method; energy conservation; structural dynamics

1. INTRODUCTION

Many time integration schemes have been developed since the early work of Newmark [1]. The Newmark time scheme family is based on a truncated Taylor series representation of the displacement field $\mathbf{u}_{n+1}$ and velocity field $\dot{\mathbf{u}}_{n+1}$ at time t_{n+1} in terms of the acceleration field $\ddot{\mathbf{u}}_{n+1}$ and the known kinematic quantities $\mathbf{u}_n$, $\dot{\mathbf{u}}_n$, and $\ddot{\mathbf{u}}_n$ at time t_n. Completed by the equation of motion expressed at time t_{n+1}, this is a system of three equations which allows to determine the three unknowns $\mathbf{u}_{n+1}$, $\dot{\mathbf{u}}_{n+1}$, and $\ddot{\mathbf{u}}_{n+1}$.

The spatial finite element discretization used in many models in structural dynamics introduces high frequency components which are not represented correctly within the discretized model and do not represent the actual behavior of the problem. However, for the Newmark time scheme

*Correspondence to: S. Krenk, Department of Mechanical Engineering, Technical University of Denmark, Building 403 Nils Koppels Alle, DK-2800 Kgs. Lyngby, Denmark.
†E-mail: sk@mek.dtu.dk

introduction of numerical damping leads to undesirable low-frequency damping and reduced order of accuracy [2]. To improve upon this situation, the so-called α-algorithms have been developed where the equation of motion is satisfied in a weighted average sense. There are three algorithms of this type, the algorithm with weighted stiffness force by Hilber *et al.* [3], the algorithm with weighted inertia forces by Wood *et al.* [4], and finally the generalized α-method of Chung and Hulbert [5] in which stiffness and inertia forces are weighted differently. Recently, it was demonstrated that the family of generalized α-methods can be obtained as special cases of a procedure in which algorithmic damping is introduced via a discretized first-order filter [6].

In the case of the Newmark scheme and the modified α-algorithms, one needs to reinterpret the energy balance equation when numerical damping is introduced. Indeed, some additional terms generated by the time discretization are added to the mechanical energy [7]. This property has motivated the development of the so-called conserving schemes that conserve the energy and momentum. The more recent literature shows a strong interest in the development of time-stepping algorithms with these conservation laws built in. One of the first representative examples in the context of non-linear elastodynamics was proposed by Simo and Tarnow [8]. Although the conservation of a physical energy is important the ability to introduce a controlled amount of dissipation in the high-frequency range is also of interest. This has led Armero and Romero to propose an algorithm which exhibits controllable numerical dissipation in the high-frequency range while ensuring conservation properties [9]. Energy conservation plays a central role when developing algorithms for contact problems and problems within multi-body dynamics and multi-domain coupling. In contact and multi-body problems the central issue is the fundamental kinematic non-linearity of the conditions for joining the bodies, see e.g. Betsch and Steinmann [10] and the references given there. In the multi-domain problems a central issue is the ability to use different time-stepping schemes in different domains, and the algorithmic damping issues associated with this.

The properties of the conservation schemes for a mechanical problem can be characterized by:

- second order or higher rate of convergence,
- exact energy balance, including conservation or controlled dissipation,
- non-linear formulation with momentum and energy balance equations,
- numerical dissipation largely concentrated in the high-frequency range, and
- algorithms can be arranged in a 'single solve' format.

It has recently been shown that the state-space formalism can be extended to include algorithmic damping in two different forms [11, 12]. In the first form dissipation is obtained by inserting suitably balanced block diagonal contributions in the state-space format. The balancing of the terms follow from an equivalence with the mechanical energy consisting of the internal energy and the kinetic energy. This scheme leads to a frequency dependence of the dissipation of the same form as in the classic Newmark algorithm, but without the energy oscillations associated with that algorithm. In the following, this version of the algorithm is referred to as the balanced dissipation scheme. This algorithm can be extended by introducing an auxiliary set of variables, defined from the displacement and velocity via first-order filters. In this way, the high-frequency behavior of the original balanced algorithm can be retained, whereas the low-frequency dissipation is reduced to higher order. In the following, this version of the algorithm is referred to as the high-frequency dissipation scheme. One can note an extension of the state-space time integration scheme for bodies with non-linear kinematics described by the Green strain tensor with momentum and energy conservation [13] and also a fourth-order accurate time integration algorithm with exact energy

DOI: 10.1002/nme

conservation for linear dynamics [14]. The considerations of the present paper can be extended in both these directions.

Efficient and accurate numerical solution is of fundamental importance for the simulation of time-dependent problems. In the presence of complex geometry or small geometric features that require locally refined meshes, the finite element methods (FEM) easily handle locally refined meshes. Adaptivity and mesh refinement are certainly keys to the efficient numerical solution of partial differential equations. As mentioned above, the spatial discretization of FEM introduces non-physical high-frequency components and it is desirable to be able to introduce a controlled energy dissipation in the high-frequency regime. Due to local mesh refinement, one must be able to control the algorithmic damping introduced locally. Furthermore, the efficiency with which the damping of the upper part of the frequency range occurs, while leaving the lower part of the frequency range undamped, is linked to the time step. Various local time-stepping schemes have been proposed, which allow smaller time steps precisely where the smallest elements in the mesh are located for example.

In the literature there are several methods for coupled analysis that use primal substructuring. Liu and Belytschko [15] outlined a coupling method thats uses element partitioning and whose stability is verified numerically. Belytschko and Mullen [16] proposed a coupling algorithm using node partitioning and they carried out a stability analysis for a time-step ratio of 1 using the energy method [17]. Daniel [18] illustrated a subcycling procedure based on a node partition using the Newmark method implemented only in terms of the displacements. The stability is proved using the conventional approach of amplification matrices showing that the stable time step depends upon the relative stiffnesses of the subdomains. Other methods [19–21] have been proposed to allow the use of different time steps in different subdomains. But multi-time-step and subcycling methods usually lead to complex procedures for time-step ratios greater than one. Moreover, the stability and accuracy analysis for such methods is substantially more involved.

Coupling methods based on the dual Schur complement approach have recently received significant attention from researchers in domain decomposition. Dual coupling methods enforce continuity of the solution across the interface between subdomains by introducing constraints that are usually imposed using Lagrange multipliers. This makes them suitable for coupling two or more subdomains almost completely independent of each other. One of the most popular and well-researched dual Schur methods is the finite element tearing and interconnecting (FETI) method proposed by Farhat and Roux [22]. The FETI method was extended for structural dynamics by Farhat *et al.* [23]. A spectral stability analysis [24] within the framework of the generalized α-method proved that the dynamic FETI algorithm is only weakly stable and predicted a linear growth instability of the decomposed problem for any constraint on the interface. Gravouil and Combescure [25, 26] extended the dynamic FETI algorithm to include multiple time steps based on the equality of velocities across the interface and proved the stability of their method using the energy method (GC method). This method has been generalized for the Newmark time integration family in linear dynamics as well as many other situations [27, 28]. Stability analysis using the energy method shows that the coupling algorithm is unconditionally stable for continuity of velocities and the critical time step for each explicit subdomain is governed by the Courant limit. Prakash and Hjelmstad [29] presented a multi-time-step coupling method for Newmark schemes which is unconditionally stable and energy preserving in the meaning of the energy method (PH method). This coupling method is built upon the multi-time-step method previously proposed by Gravouil and Combescure. In the case of a single time step in all the subdomains, the GC method and the PH method are energy preserving in that they do not add or remove energy from the coupled

DOI: 10.1002/nme

system. Otherwise, for multi-time-step cases the GC method is dissipative, whereas the PH method is shown to be energy preserving for general multi-time-step cases.

The present work proposes a dual Schur complement method that allows coupling of subdomains with independent numerical dissipation parameters and with independent time steps. The method ensures zero interface dissipation by construction. The first part describes the introduction of the Lagrange multipliers in the balanced and high-frequency dissipation scheme for a single domain. A general algorithm is presented and arranged in a 'single-solve' format. In the second part, the coupling method is presented in two steps: first with independent numerical dissipation parameters and then with independent time steps. Global stability of the method is demonstrated by an energy balance equation which shows that the work of the interface forces is identically zero. General algorithms are presented to illustrate the coupling of two subdomains integrated with different dissipation parameters and different time steps. In the last section, a 2D example is presented illustrating the accuracy and efficiency of the proposed approach.

2. STATE-SPACE SCHEME WITH ENERGY DISSIPATION AND CONSTRAINTS

Consider a domain Ω with prescribed displacement on a portion of its boundary Γ_u and prescribed tractions on the remaining boundary Γ_t. Using a finite element discretization in space, the semi-discretized equations for a damped system with linear elastic relationships can be written as:

$$\mathbf{M}\ddot{\mathbf{u}}(t)+\mathbf{C}\dot{\mathbf{u}}(t)+\mathbf{K}\mathbf{u}(t)=\mathbf{f}(t), \tag{1}$$

$$\mathbf{u}(0)=\mathbf{u}_0, \quad \dot{\mathbf{u}}(0)=\dot{\mathbf{u}}_0, \tag{2}$$

$$\mathbf{u}(t)=\mathbf{u}_d(t) \quad \text{on } \Gamma_u. \tag{3}$$

Here $\mathbf{M}$ represents the mass matrix, $\mathbf{C}$ the viscous damping matrix, and $\mathbf{K}$ the stiffness matrix, here assumed to be constant. The nodal displacement is noted as $\mathbf{u}(t)$ and $\mathbf{f}(t)$ is the external forces vector at time t. $\mathbf{u}_0$ and $\dot{\mathbf{u}}_0$ are the specified initial displacement and velocity vectors, respectively, whereas $\mathbf{u}_d(t)$ is the displacement boundary condition on Γ_u at time t. If Lagrange multipliers are employed to enforce the prescribed displacement (3) on the boundary Γ_u, the equation of motion (1) is modified as

$$\mathbf{M}\ddot{\mathbf{u}}(t)+\mathbf{C}\dot{\mathbf{u}}(t)+\mathbf{K}\mathbf{u}(t)=\mathbf{f}(t)-\mathbf{L}^{\mathrm{T}}\boldsymbol{\lambda}(t), \tag{4}$$

$$\mathbf{L}\mathbf{u}(t)=\mathbf{L}\mathbf{u}_d(t), \tag{5}$$

where $\boldsymbol{\lambda}$ is a vector of Lagrange multipliers representing the traction forces at the boundary Γ_u, and $\mathbf{L}$ is a boolean matrix which localizes the boundary degrees of freedom of the domain Ω. Equation (5) expresses the constraint on the displacement at the boundary Γ_u. The superscript 'T' denotes the transpose of a quantity.

The second-order differential equations of dynamics (4) and (5) are recast into an augmented set of first-order differential equations by introduction of a new independent variable representing the velocity $\mathbf{v}=\dot{\mathbf{u}}$. By multiplication of this last relation with the mass matrix $\mathbf{M}$, the augmented

DOI: 10.1002/nme

system takes a symmetric form in terms of the state-space variables $[\mathbf{u}^{\mathrm{T}}, \mathbf{v}^{\mathrm{T}}, \boldsymbol{\lambda}^{\mathrm{T}}]$:

$$\begin{bmatrix} \mathbf{C} & \mathbf{M} & \mathbf{0} \\ \mathbf{M} & \mathbf{0} & \mathbf{0} \\ \mathbf{0} & \mathbf{0} & \mathbf{0} \end{bmatrix} \begin{bmatrix} \dot{\mathbf{u}} \\ \dot{\mathbf{v}} \\ \mathbf{0} \end{bmatrix} + \begin{bmatrix} \mathbf{K} & \mathbf{0} & \mathbf{L}^{\mathrm{T}} \\ \mathbf{0} & -\mathbf{M} & \mathbf{0} \\ \mathbf{L} & \mathbf{0} & \mathbf{0} \end{bmatrix} \begin{bmatrix} \mathbf{u} \\ \mathbf{v} \\ \boldsymbol{\lambda} \end{bmatrix} = \begin{bmatrix} \mathbf{f}(t) \\ \mathbf{0} \\ \mathbf{L}\mathbf{u}_d(t) \end{bmatrix}. \tag{6}$$

The state-space equation (6) is integrated over the time interval $[t_n, t_{n+1}]$. The first term in Equation (6) is integrated exactly, whereas the second term contains integrals of the displacement, velocity, and Lagrange multipliers over the time interval $[t_n, t_{n+1}]=[t_n, t_n+h]$. The time mean value over the time interval is denoted by an overbar, e.g. $\bar{\mathbf{f}}=h^{-1}\int_n^{n+1}\mathbf{f}\,\mathrm{d}t$, whereby the integrated state-space equations take the form

$$\begin{bmatrix} \mathbf{C} & \mathbf{M} & \mathbf{0} \\ \mathbf{M} & \mathbf{0} & \mathbf{0} \\ \mathbf{0} & \mathbf{0} & \mathbf{0} \end{bmatrix} \begin{bmatrix} \Delta\mathbf{u} \\ \Delta\mathbf{v} \\ \mathbf{0} \end{bmatrix} + h \begin{bmatrix} \mathbf{K} & \mathbf{0} & \mathbf{L}^{\mathrm{T}} \\ \mathbf{0} & -\mathbf{M} & \mathbf{0} \\ \mathbf{L} & \mathbf{0} & \mathbf{0} \end{bmatrix} \begin{bmatrix} \bar{\mathbf{u}} \\ \bar{\mathbf{v}} \\ \bar{\boldsymbol{\lambda}} \end{bmatrix} = \begin{bmatrix} h\bar{\mathbf{f}} \\ \mathbf{0} \\ h\mathbf{L}\bar{\mathbf{u}}_d \end{bmatrix}, \tag{7}$$

where $\Delta\mathbf{u}$ and $\Delta\mathbf{v}$ are the finite increments over the time interval:

$$\Delta\mathbf{u}=\mathbf{u}_{n+1}-\mathbf{u}_n \quad \text{and} \quad \Delta\mathbf{v}=\mathbf{v}_{n+1}-\mathbf{v}_n. \tag{8}$$

The time integrals of the displacement and velocity vectors are generally unknown. $\bar{\mathbf{u}}$ and $\bar{\mathbf{v}}$ can be expressed as the mean value for linear problems and second-order accurate schemes as

$$\bar{\mathbf{u}}=\tfrac{1}{2}(\mathbf{u}_{n+1}+\mathbf{u}_n) \quad \text{and} \quad \bar{\mathbf{v}}=\tfrac{1}{2}(\mathbf{v}_{n+1}+\mathbf{v}_n). \tag{9}$$

The Lagrange multipliers λ are initially unknown and only appear in the discretized equation of motion through their time integrals, represented by the mean value vector

$$\bar{\boldsymbol{\lambda}}=\frac{1}{h}\int_n^{n+1}\boldsymbol{\lambda}(t)\,\mathrm{d}t. \tag{10}$$

It should be noted that in the discretized equations the Lagrange multiplier enters only via the mean value $\bar{\boldsymbol{\lambda}}$, generated via the integration of the equations over the time increment.

The following section briefly summarizes the balanced dissipation scheme [11, 12] where the introduction of two balanced dissipation terms give monotonic frequency dependence (Section 2.1). Then the extension to high-frequency damping by introduction of extended state-space variables is summarized (Section 2.2). In both cases the focus is on the introduction of the Lagrange multipliers $\boldsymbol{\lambda}$ and the establishment of the corresponding energy balance equations.

2.1. Balanced dissipation scheme

As suggested in [11, 12], algorithmic damping can be obtained by introducing terms in the diagonal of the first matrix of the integrated state-space equation (7). For a linear system without damping, this leads to the following form:

$$\begin{bmatrix} \frac{1}{2}\alpha h\mathbf{K} & \mathbf{M} & \mathbf{0} \\ \mathbf{M} & -\frac{1}{2}\alpha h\mathbf{M} & \mathbf{0} \\ \mathbf{0} & \mathbf{0} & \mathbf{0} \end{bmatrix} \begin{bmatrix} \Delta\mathbf{u} \\ \Delta\mathbf{v} \\ \mathbf{0} \end{bmatrix} + h \begin{bmatrix} \mathbf{K} & \mathbf{0} & \mathbf{L}^{\mathrm{T}} \\ \mathbf{0} & -\mathbf{M} & \mathbf{0} \\ \mathbf{L} & \mathbf{0} & \mathbf{0} \end{bmatrix} \begin{bmatrix} \bar{\mathbf{u}} \\ \bar{\mathbf{v}} \\ \bar{\boldsymbol{\lambda}} \end{bmatrix} = \begin{bmatrix} h\bar{\mathbf{f}} \\ \mathbf{0} \\ h\mathbf{L}\bar{\mathbf{u}}_d \end{bmatrix}. \tag{11}$$

DOI: 10.1002/nme

The energy balance equation is obtained by pre-multiplication of (11) with $[\Delta\mathbf{u}^{\mathrm{T}}, -\Delta\mathbf{v}^{\mathrm{T}}, \mathbf{0}^{\mathrm{T}}]$:

$$\left[\tfrac{1}{2}\mathbf{v}^{\mathrm{T}}\mathbf{M}\mathbf{v}+\tfrac{1}{2}\mathbf{u}^{\mathrm{T}}\mathbf{K}\mathbf{u}\right]_n^{n+1} = \Delta\mathbf{u}^{\mathrm{T}}\bar{\mathbf{f}} - \Delta\mathbf{u}^{\mathrm{T}}\mathbf{L}^{\mathrm{T}}\bar{\boldsymbol{\lambda}} - \tfrac{1}{2}\alpha(\Delta\mathbf{u}^{\mathrm{T}}\mathbf{K}\Delta\mathbf{u}+\Delta\mathbf{v}^{\mathrm{T}}\mathbf{M}\Delta\mathbf{v}). \tag{12}$$

The scheme is seen to be stable in the energy norm for $\alpha \geqslant 0$, and to be dissipative for $\alpha > 0$. A spectral analysis of the basic form without Lagrange multipliers was given in [11]. It is noted that the contribution of the interface forces, $\Delta\mathbf{u}^{\mathrm{T}}\mathbf{L}^{\mathrm{T}}\bar{\boldsymbol{\lambda}}$, to the energy balance equation (12) is similar to that of the external forces.

2.2. *High-frequency dissipation scheme*

The high-frequency damping formulation of the state-space algorithm [11] is obtained by replacing the diagonal terms in the first matrix of (11) in terms of $\Delta\mathbf{u}$ and $\Delta\mathbf{v}$ with similar increments of two new auxiliary variables $\mathbf{s}$ and $\mathbf{t}$. These variables are defined by a discretized form of the filter equations

$$\begin{aligned} \alpha h\dot{\mathbf{s}}+\mathbf{s} &= h\dot{\mathbf{u}}, \\ \alpha h\dot{\mathbf{t}}+\mathbf{t} &= h\dot{\mathbf{v}}. \end{aligned} \tag{13}$$

In the low- and mid-frequency regime, the new variables $\mathbf{s}$ and $\mathbf{t}$ are roughly equivalent to $h\dot{\mathbf{u}}$ and $h\dot{\mathbf{v}}$, which will make their contribution to the dissipation small in this frequency range.

When the increments $\Delta\mathbf{u}$ and $\Delta\mathbf{v}$ in the damping terms in Equation (11) are replaced by the increments $\frac{1}{2}\alpha\Delta\mathbf{s}$ and $\frac{1}{2}\alpha\Delta\mathbf{t}$ of the corresponding filtered variables, the resulting equations of motion for a linear system without damping take the form

$$\begin{bmatrix} \mathbf{0} & \mathbf{M} & \mathbf{0} \\ \mathbf{M} & \mathbf{0} & \mathbf{0} \\ \mathbf{0} & \mathbf{0} & \mathbf{0} \end{bmatrix} \begin{bmatrix} \Delta\mathbf{u} \\ \Delta\mathbf{v} \\ \mathbf{0} \end{bmatrix} + h \begin{bmatrix} \mathbf{K} & \mathbf{0} & \mathbf{L}^{\mathrm{T}} \\ \mathbf{0} & -\mathbf{M} & \mathbf{0} \\ \mathbf{L} & \mathbf{0} & \mathbf{0} \end{bmatrix} \begin{bmatrix} \bar{\mathbf{u}} \\ \bar{\mathbf{v}} \\ \bar{\boldsymbol{\lambda}} \end{bmatrix} + \frac{\alpha^2 h}{4} \begin{bmatrix} \mathbf{K} & \mathbf{0} & \mathbf{0} \\ \mathbf{0} & -\mathbf{M} & \mathbf{0} \\ \mathbf{0} & \mathbf{0} & \mathbf{0} \end{bmatrix} \begin{bmatrix} \Delta\mathbf{s} \\ \Delta\mathbf{t} \\ \mathbf{0} \end{bmatrix} = \begin{bmatrix} h\bar{\mathbf{f}} \\ \mathbf{0} \\ h\mathbf{L}\bar{\mathbf{u}}_d \end{bmatrix} \tag{14}$$

supplemented by the discretized filter equations

$$\alpha \begin{bmatrix} \Delta\mathbf{s} \\ \Delta\mathbf{t} \end{bmatrix} + \begin{bmatrix} \bar{\mathbf{s}} \\ \bar{\mathbf{t}} \end{bmatrix} = \begin{bmatrix} \Delta\mathbf{u} \\ \Delta\mathbf{v} \end{bmatrix} \tag{15}$$

for the auxiliary variables $\mathbf{s}$ and $\mathbf{t}$.

The energy balance equation is obtained by pre-multiplying equation (14) with $[\Delta\mathbf{u}^{\mathrm{T}}, -\Delta\mathbf{v}^{\mathrm{T}}, \mathbf{0}^{\mathrm{T}}]$ and (15) with $[\Delta\mathbf{s}^{\mathrm{T}}, -\Delta\mathbf{t}^{\mathrm{T}}]$. Combination gives the energy balance equation

$$\left[\tfrac{1}{2}\mathbf{v}^{\mathrm{T}}\mathbf{M}\mathbf{v}+\tfrac{1}{2}\mathbf{u}^{\mathrm{T}}\mathbf{K}\mathbf{u}+\tfrac{1}{8}\alpha^2(\mathbf{t}^{\mathrm{T}}\mathbf{M}\mathbf{t}+\mathbf{s}^{\mathrm{T}}\mathbf{K}\mathbf{s})\right]_n^{n+1} = \Delta\mathbf{u}^{\mathrm{T}}\bar{\mathbf{f}} - \Delta\mathbf{u}^{\mathrm{T}}\mathbf{L}^{\mathrm{T}}\bar{\boldsymbol{\lambda}} - \tfrac{1}{4}\alpha^3(\Delta\mathbf{s}^{\mathrm{T}}\mathbf{K}\Delta\mathbf{s}+\Delta\mathbf{t}^{\mathrm{T}}\mathbf{M}\Delta\mathbf{t}). \tag{16}$$

The coefficient α leads to high-frequency energy dissipation, when positive. The detailed behavior is determined by a spectral analysis in [11]. The energy balance equation (16) demonstrates the unconditional stability of the scheme for $\alpha \geqslant 0$. As for the balanced dissipation scheme the contribution of the interface $\Delta\mathbf{u}^{\mathrm{T}}\mathbf{L}^{\mathrm{T}}\bar{\boldsymbol{\lambda}}$ is similar to that of the external forces.

DOI: 10.1002/nme

3. STATE-SPACE ALGORITHMS WITH LINEAR CONSTRAINTS

In this section, a general form of the extended state-space scheme is presented to facilitate the derivation of the present multi-time-step coupling method. Both variants of the state-space scheme (Equations (11) and (14)–(15)) with linear constraint can be put on the following form:

$$\begin{bmatrix} \mathbb{K}^* & \mathbb{L}^{\mathrm{T}} \\ \mathbb{L} & \mathbf{0} \end{bmatrix} \begin{bmatrix} \Delta\mathbb{U} \\ \bar{\mathbf{\Lambda}} \end{bmatrix} = \begin{bmatrix} \mathbb{F} \\ 2\mathbb{L}\mathbb{U}_* \end{bmatrix} - \begin{bmatrix} \mathbb{N} & \mathbf{0} \\ 2\mathbb{L} & \mathbf{0} \end{bmatrix} \begin{bmatrix} \mathbb{U}_n \\ \mathbf{0} \end{bmatrix}. \tag{17}$$

The equation system (17) is symmetric, but not positive-definite because of the zeros on the lower part of the diagonal. Equation (17) is solved by using a bordering approach [30] that can be seen as a predictor-corrector method. The Lagrange multiplier $\bar{\mathbf{\Lambda}}$ is determined by forming a linear combination of the two equations with the first equation pre-multiplied by $\mathbb{L}[\mathbb{K}^*]^{-1}$ and the second by -1:

$$\bar{\mathbf{\Lambda}} = \mathbb{H}^{-1}\{\mathbb{L}\Delta\tilde{\mathbb{U}} + 2\mathbb{L}\mathbb{U}_n - 2\mathbb{L}\mathbb{U}_*\} \quad \text{with } \mathbb{H} = [\mathbb{L}[\mathbb{K}^*]^{-1}\mathbb{L}^{\mathrm{T}}]. \tag{18}$$

In Equation (18), the term $\Delta\tilde{\mathbb{U}}$ is defined as the predictor of the displacement increment $\Delta\mathbb{U}$ as given by the solution of the free motion equation:

$$\Delta\tilde{\mathbb{U}} = [\mathbb{K}^*]^{-1}\{\mathbb{F} - \mathbb{N}\mathbb{U}_n\}. \tag{19}$$

Knowing the predictor value of the displacement increment $\Delta\tilde{\mathbb{U}}$, the mean value of the Lagrange multipliers $\bar{\mathbf{\Lambda}}$ can be calculated by Equation (18). The corrector of the displacement increment $\Delta\breve{\mathbb{U}}$, which can be interpreted as the solution of the link motion, is then calculated as

$$\Delta\breve{\mathbb{U}} = -[\mathbb{K}^*]^{-1}\{\mathbb{L}^{\mathrm{T}}\bar{\mathbf{\Lambda}}\}. \tag{20}$$

Finally, the displacement increment $\Delta\mathbb{U}$ is found by addition of predictor and corrector:

$$\Delta\mathbb{U} = \Delta\breve{\mathbb{U}} + \Delta\tilde{\mathbb{U}}. \tag{21}$$

Thus, to solve system (17) the predictor $\Delta\tilde{\mathbb{U}}$ is first computed from Equation (19), then $\bar{\mathbf{\Lambda}}$ is determined from Equation (18), and finally the displacement solution is found by including the corrector $\Delta\breve{\mathbb{U}}$ from Equation (20).

A more compact and uniform format of the two algorithms can be obtained by introducing a parameter κ, defined in terms of α as shown in Table I, [11]. This leads to an effective stiffness matrix $\mathbf{K}^*$ defined as

$$\mathbf{K}^* = \kappa\left[\mathbf{K} + \frac{2}{\kappa h}\mathbf{C} + \left(\frac{2}{\kappa h}\right)^2\mathbf{M}\right]. \tag{22}$$

The vectors and matrices which appear in Equation (17) are presented in Tables II and III for both versions of the algorithm. The general algorithms for the balanced dissipation scheme and the

Table I. Algorithmic damping parameter κ.

	Balanced dissipation	High-frequency dissipation
κ	$1+\alpha$	$1+\dfrac{\alpha^2}{(1+2\alpha)}$

DOI: 10.1002/nme

Table II. General vectors $\mathbb{F}$, $\mathbb{U}_n$, $\Delta\mathbb{U}$, $\mathbb{U}_*$, and $\bar{\mathbf{\Lambda}}$.

	Balanced dissipation	High-frequency dissipation
$\mathbb{F}^{\mathrm{T}}$	$[\bar{\mathbf{f}}^{\mathrm{T}}\ \mathbf{0}]$	$[\bar{\mathbf{f}}^{\mathrm{T}}\ \mathbf{0}\ \mathbf{0}\ \mathbf{0}]$
$\mathbb{U}_n^{\mathrm{T}}$	$[\mathbf{u}_n^{\mathrm{T}}\ \mathbf{v}_n^{\mathrm{T}}]$	$[\mathbf{u}_n^{\mathrm{T}}\ \mathbf{v}_n^{\mathrm{T}}\ \mathbf{s}_n^{\mathrm{T}}\ \mathbf{t}_n^{\mathrm{T}}]$
$\Delta\mathbb{U}^{\mathrm{T}}$	$[\Delta\mathbf{u}^{\mathrm{T}}\ \Delta\mathbf{v}^{\mathrm{T}}]$	$[\Delta\mathbf{u}^{\mathrm{T}}\ \Delta\mathbf{v}^{\mathrm{T}}\ \Delta\mathbf{s}^{\mathrm{T}}\ \Delta\mathbf{t}^{\mathrm{T}}]$
$\mathbb{U}_*^{\mathrm{T}}$	$[\bar{\mathbf{u}}_d^{\mathrm{T}}\ \mathbf{0}]$	$[\bar{\mathbf{u}}_d^{\mathrm{T}}\ \mathbf{0}\ \mathbf{0}\ \mathbf{0}]$
$\bar{\mathbf{\Lambda}}^{T}$	$[2\bar{\boldsymbol{\lambda}}^{\mathrm{T}}\ \mathbf{0}]$	$[2\bar{\boldsymbol{\lambda}}^{\mathrm{T}}\ \mathbf{0}\ \mathbf{0}\ \mathbf{0}]$

Table III. General matrices $\mathbb{K}^*$, $\mathbb{N}$, and $\mathbb{L}$.

	Balanced dissipation	High-frequency dissipation
$\mathbb{K}^*$	$\begin{bmatrix} \mathbf{K}^* & \mathbf{0} \\ -\frac{2}{\kappa h}\mathbf{I} & \mathbf{I} \end{bmatrix}$	$\begin{bmatrix} \mathbf{K}^* & \mathbf{0} & \mathbf{0} & \mathbf{0} \\ -\frac{2}{\kappa h}\mathbf{I} & \mathbf{I} & \mathbf{0} & \mathbf{0} \\ -\frac{1}{\frac{1}{2}+\alpha}\mathbf{I} & \mathbf{0} & \mathbf{I} & \mathbf{0} \\ \mathbf{0} & -\frac{1}{\frac{1}{2}+\alpha}\mathbf{I} & \mathbf{0} & \mathbf{I} \end{bmatrix}$
$\mathbb{N}$	$\begin{bmatrix} 2\mathbf{K} & -\frac{4}{\kappa h}\mathbf{M} \\ \mathbf{0} & \frac{2}{\kappa}\mathbf{I} \end{bmatrix}$	$\begin{bmatrix} 2\mathbf{K} & -\frac{4}{\kappa h}\mathbf{M} & -(\kappa-1)\mathbf{K} & \frac{2}{\kappa h}(\kappa-1)\mathbf{M} \\ \mathbf{0} & \frac{2}{\kappa h}\mathbf{I} & \mathbf{0} & \mathbf{0} \\ \mathbf{0} & \mathbf{0} & \left(\frac{1}{2}+\alpha\right)^{-1}\mathbf{I} & \mathbf{0} \\ \mathbf{0} & \mathbf{0} & \mathbf{0} & \left(\frac{1}{2}+\alpha\right)^{-1}\mathbf{I} \end{bmatrix}$
$\mathbb{L}^{\mathrm{T}}$	$[\mathbf{L}^{\mathrm{T}}\ \mathbf{0}]$	$[\mathbf{L}^{\mathrm{T}}\ \mathbf{0}\ \mathbf{0}\ \mathbf{0}]$

high-frequency scheme for linear systems including structural damping and with linear constraint are presented, respectively, in Tables IV and V. In Table III, $\mathbf{I}$ is an identity matrix of dimension N, the size of the domain.

4. SUBDOMAIN COUPLING IN DYNAMICS

In the previous section, Lagrange multipliers were introduced in the state-space scheme in order to take constraints explicitly into account. In this section a multi-time-step coupling method is

DOI: 10.1002/nme

Table IV. Balanced state-space algorithm with linear constraint.

(1) System matrices: $\mathbf{M}$, $\mathbf{C}$, $\mathbf{K}$, $\mathbf{L}$

$$\kappa = 1+\alpha$$

$$\mathbf{K}^* = \kappa\left[\mathbf{K} + \tfrac{2}{\kappa h}\mathbf{C} + \left(\tfrac{2}{\kappa h}\right)^2\mathbf{M}\right]$$

$$\mathbf{H} = \mathbf{L}[\mathbf{K}^*]^{-1}\mathbf{L}^{\mathrm{T}}$$

(2) Initial conditions: $\mathbf{u}_0$, $\mathbf{v}_0$

(3) Increment: $t_{n+1} = t_n + h$

$$\Delta\tilde{\mathbf{u}} = [\mathbf{K}^*]^{-1}\left\{2\bar{\mathbf{f}} - 2\mathbf{K}\mathbf{u}_n + \tfrac{4}{\kappa h}\mathbf{M}\mathbf{v}_n\right\} \text{ and } \Delta\tilde{\mathbf{v}} = \tfrac{2}{\kappa h}\Delta\tilde{\mathbf{u}} - \tfrac{2}{\kappa}\mathbf{v}_n$$

$$2\bar{\boldsymbol{\lambda}} = \mathbf{H}^{-1}\{\mathbf{L}\Delta\tilde{\mathbf{u}} + 2\mathbf{L}\mathbf{u}_n - 2\mathbf{L}\bar{\mathbf{u}}_d\}$$

$$\Delta\check{\mathbf{u}} = -[\mathbf{K}^*]^{-1}\{2\mathbf{L}^{\mathrm{T}}\bar{\boldsymbol{\lambda}}\} \text{ and } \Delta\check{\mathbf{v}} = \tfrac{2}{\kappa h}\Delta\check{\mathbf{u}}$$

(4) Vector increment update:

$$\Delta\mathbf{u} = \Delta\tilde{\mathbf{u}} + \Delta\check{\mathbf{u}} \text{ and } \Delta\mathbf{v} = \Delta\tilde{\mathbf{v}} + \Delta\check{\mathbf{v}}$$

(5) Vector update:

$$\mathbf{u}_{n+1} = \mathbf{u}_n + \Delta\mathbf{u} \text{ and } \mathbf{v}_{n+1} = \mathbf{v}_n + \Delta\mathbf{v}$$

(6) Return to (3) for next time step, or stop

presented using a dual Schur domain decomposition method. This method allows to divide a large structural mesh into a number of smaller subdomains. Each subdomain is solved independently and coupled to obtain the solution of the original problem. The various subdomains can be integrated in time using different time scale and/or different algorithmic damping parameter κ of the state-space schemes. The kinematic continuity condition between the subdomains is derived from the condition that the interface should not contribute directly to the energy balance equation. Consider a continuous problem domain Ω which is decomposed into s subdomains Ω_k for $k \in [1 \ldots s]$ as shown in Figure 1(a). This partitioning creates the interface Γ_b of shared nodes between the subdomains. Let the number of degrees of freedom in subdomain Ω_k be N_k and the total number of degrees of freedom along Γ_b be L. As shown in Figure 1(b), there are additional forces $\mathbf{f}^{\mathrm{link}}(t)$ acting on a subdomain resulting from its interaction with the rest of the mesh. In Section 4.1 the coupling method is derived for the case where two subdomains have the identical time scale and different κ parameters. In Section 4.2 the coupling method is derived for the case where two subdomains have individual time scales and different κ parameters. In the following, the high-frequency dissipation scheme is illustrated for identical time steps, whereas the balanced dissipation scheme is used to illustrate the use of different time steps. Evidently, either of the schemes can be employed in each of the two cases.

4.1. Domain decomposition with common time step and individual damping parameters

In this section two subdomains A and B are integrated in time with the high-frequency dissipation scheme with individual κ parameters and identical time step as illustrated in Figure 2. According to Equation (16) the global energy balance equation over a time interval $[t_n, t_{n+1} = t_n + h]$ can be

DOI: 10.1002/nme

Table V. High-frequency state-space algorithm with linear constraint.

(1) System matrices $\mathbf{M}$, $\mathbf{C}$, $\mathbf{K}$, $\mathbf{L}$

$\kappa = 1 + \frac{\alpha^2}{(1+2\alpha)}$

$\mathbf{K}^* = \kappa[\mathbf{K} + \frac{2}{\kappa h}\mathbf{C} + (\frac{2}{\kappa h})^2\mathbf{M}]$

$\mathbf{H} = \mathbf{L}[\mathbf{K}^*]^{-1}\mathbf{L}^{\mathrm{T}}$

(2) Initial conditions: $\mathbf{u}_0$, $\mathbf{v}_0$

$\mathbf{s}_0 = \mathbf{0}$, $\mathbf{t}_0 = \mathbf{0}$

(3) Increment: $t_{n+1} = t_n + h$

$\Delta\tilde{\mathbf{u}} = [\mathbf{K}^*]^{-1}\{2\bar{\mathbf{f}} - \mathbf{K}[2\mathbf{u}_n - (\kappa-1)\mathbf{s}_n] + \frac{2}{\kappa h}\mathbf{M}[2\mathbf{v}_n - (\kappa-1)\mathbf{t}_n]\}$

$\Delta\tilde{\mathbf{v}} = \frac{2}{\kappa h}\Delta\tilde{\mathbf{u}} - \frac{1}{\kappa}[2\mathbf{v}_n - (\kappa-1)\mathbf{t}_n]$

$\Delta\tilde{\mathbf{s}} = (\frac{1}{2}+\alpha)^{-1}(\Delta\tilde{\mathbf{u}} - \mathbf{s}_n)$ and $\Delta\tilde{\mathbf{t}} = (\frac{1}{2}+\alpha)^{-1}(\Delta\tilde{\mathbf{v}} - \mathbf{t}_n)$

$2\bar{\boldsymbol{\lambda}} = \mathbf{H}^{-1}\{\mathbf{L}\Delta\tilde{\mathbf{u}} + 2\mathbf{L}\mathbf{u}_n - 2\mathbf{L}\bar{\mathbf{u}}_d\}$

$\Delta\check{\mathbf{u}} = -[\mathbf{K}^*]^{-1}\{2\mathbf{L}^{\mathrm{T}}\bar{\boldsymbol{\lambda}}\}$ and $\Delta\check{\mathbf{v}} = \frac{2}{\kappa h}\Delta\check{\mathbf{u}}$

$\Delta\check{\mathbf{s}} = (\frac{1}{2}+\alpha)^{-1}\Delta\check{\mathbf{u}}$ and $\Delta\check{\mathbf{t}} = (\frac{1}{2}+\alpha)^{-1}\Delta\check{\mathbf{v}}$

(4) Vector increment update:

$\Delta\mathbf{u} = \Delta\tilde{\mathbf{u}} + \Delta\check{\mathbf{u}}$ and $\Delta\mathbf{v} = \Delta\tilde{\mathbf{v}} + \Delta\check{\mathbf{v}}$

$\Delta\mathbf{s} = \Delta\tilde{\mathbf{s}} + \Delta\check{\mathbf{s}}$ and $\Delta\mathbf{t} = \Delta\tilde{\mathbf{t}} + \Delta\check{\mathbf{t}}$

(5) Vector update:

$\mathbf{u}_{n+1} = \mathbf{u}_n + \Delta\mathbf{u}$ and $\mathbf{v}_{n+1} = \mathbf{v}_n + \Delta\mathbf{v}$

$\mathbf{s}_{n+1} = \mathbf{s}_n + \Delta\mathbf{s}$ and $\mathbf{t}_{n+1} = \mathbf{t}_n + \Delta\mathbf{t}$

(6) Return to (3) for next time step, or stop

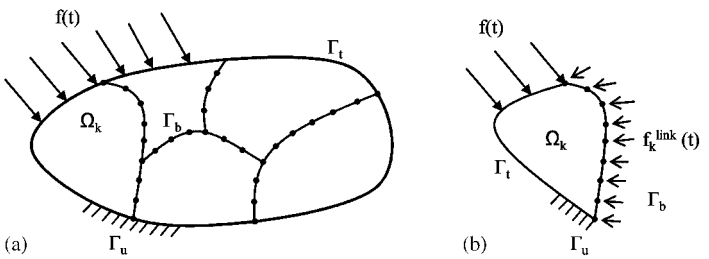

Figure 1. Model problem: (a) partitioned domain showing shared nodes and (b) a typical subdomain.

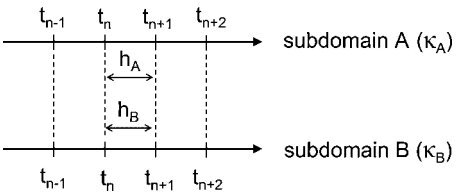

Figure 2. Subdomains A and B integrated with different κ parameter and identical time step.

DOI: 10.1002/nme

written as

$$\left[\tfrac{1}{2}\mathbf{v}_A^{\mathrm{T}}\mathbf{M}_A\mathbf{v}_A+\tfrac{1}{2}\mathbf{u}_A^{\mathrm{T}}\mathbf{K}_A\mathbf{u}_A+\tfrac{1}{8}\alpha_A^2(\mathbf{t}_A^{\mathrm{T}}\mathbf{M}_A\mathbf{t}_A+\mathbf{s}_A^{\mathrm{T}}\mathbf{K}_A\mathbf{s}_A)\right]_n^{n+1}$$

$$+\left[\tfrac{1}{2}\mathbf{v}_B^{\mathrm{T}}\mathbf{M}_B\mathbf{v}_B+\tfrac{1}{2}\mathbf{u}_B^{\mathrm{T}}\mathbf{K}_B\mathbf{u}_B+\tfrac{1}{8}\alpha_B^2(\mathbf{t}_B^{\mathrm{T}}\mathbf{M}_B\mathbf{t}_B+\mathbf{s}_B^{\mathrm{T}}\mathbf{K}_B\mathbf{s}_B)\right]_n^{n+1}$$

$$=\Delta\mathbf{u}_A^{\mathrm{T}}\mathbf{L}_A^{\mathrm{T}}\bar{\boldsymbol{\lambda}}-\tfrac{1}{4}\alpha_A^3(\Delta\mathbf{s}_A^{\mathrm{T}}\mathbf{K}_A\Delta\mathbf{s}_A+\Delta\mathbf{t}_A^{\mathrm{T}}\mathbf{M}_A\Delta\mathbf{t}_A)$$

$$+\Delta\mathbf{u}_B^{\mathrm{T}}\mathbf{L}_B^{\mathrm{T}}\bar{\boldsymbol{\lambda}}-\tfrac{1}{4}\alpha_B^3(\Delta\mathbf{s}_B^{\mathrm{T}}\mathbf{K}_B\Delta\mathbf{s}_B+\Delta\mathbf{t}_B^{\mathrm{T}}\mathbf{M}_B\Delta\mathbf{t}_B). \tag{23}$$

The energy balance equation of the initial domain Ω is obtained by summing the contribution of the two domains Ω_A and Ω_B. The work at the interface between the two subdomains due to the coupling method is identified as

$$\Delta W_{\mathrm{inter}}=\Delta\mathbf{u}_A^{\mathrm{T}}\mathbf{L}_A^{\mathrm{T}}\bar{\lambda}+\Delta\mathbf{u}_B^{\mathrm{T}}\mathbf{L}_B^{\mathrm{T}}\bar{\lambda}. \tag{24}$$

This expression clearly identifies the parameter $\bar{\lambda}$ as the 'representative force' acting through the displacement increment $\Delta\mathbf{u}$ over the considered time interval h.

The condition is now imposed that the interface does not contribute to the energy balance, i.e $W_{\mathrm{inter}}=0$. It then follows from (24), one has to impose that $\mathbf{L}_A\Delta\mathbf{u}_A+\mathbf{L}_B\Delta\mathbf{u}_B=\mathbf{0}$. The displacements are assumed to be continuous at the interface between the subdomains at the initial time. And thus, this is equivalent to imposing the continuity condition in the form

$$\mathbf{L}_A\mathbf{u}_k^A+\mathbf{L}_B\mathbf{u}_k^B=\mathbf{0}\quad\forall k\in\{1,2,\ldots,n,\ldots\}. \tag{25}$$

Here and in the following the indices, such as A and B, are placed such as best to allow other indices, and thus may sometimes appear as superscripts.

One can present on a general matrix form the coupling of two subdomains with identical time step and different κ parameters as:

$$\begin{bmatrix}\mathbb{K}_A^* & \mathbf{0} & \mathbb{L}_A^{\mathrm{T}}\\ \mathbf{0} & \mathbb{K}_B^* & \mathbb{L}_B^{\mathrm{T}}\\ \mathbb{L}_A & \mathbb{L}_B & \mathbf{0}\end{bmatrix}\begin{bmatrix}\Delta\mathbb{U}_A\\ \Delta\mathbb{U}_B\\ \bar{\boldsymbol{\Lambda}}\end{bmatrix}=\begin{bmatrix}\mathbb{F}_A\\ \mathbb{F}_B\\ \mathbf{0}\end{bmatrix}-\begin{bmatrix}\mathbb{N}_A & \mathbf{0} & \mathbf{0}\\ \mathbf{0} & \mathbb{N}_B & \mathbf{0}\\ 2\mathbb{L}_A & 2\mathbb{L}_B & \mathbf{0}\end{bmatrix}\begin{bmatrix}\mathbb{U}_n^A\\ \mathbb{U}_n^B\\ \mathbf{0}\end{bmatrix}. \tag{26}$$

The general algorithm with high-frequency dissipation in both subdomains is presented in Table VI for a time step from t_n to t_{n+1}. This method can be extended to any number of subdomains with individual κ parameters and time integration with identical time step.

4.2. Domain decomposition with individual time steps and individual damping parameters

In this section two subdomains A and B are integrated in time with the balanced dissipation scheme: individual κ parameters and time step illustrated in Figure 3. The time scale on the subdomain A is referred as the coarse time scale and on the subdomain B as the micro time scale. According to Equation (16), the global energy balance equation over a time interval $[t_0, t_m=t_0+h_A]$ of the

DOI: 10.1002/nme

Table VI. Coupling two subdomains with identical time step and different numerical schemes.

(1) System matrices

$\mathbf{K}_A,\ \mathbf{C}_A,\ \mathbf{M}_A,\ \mathbf{L}_A,\ \alpha_A$	$\mathbf{K}_B,\ \mathbf{C}_B,\ \mathbf{M}_B,\ \mathbf{L}_B,\ \alpha_B$
$\kappa_A = 1 + \frac{\alpha_A^2}{(1+2\alpha_A)}$	$\kappa_B = 1 + \frac{\alpha_B^2}{(1+2\alpha_B)}$
$\mathbf{K}_A^* = \kappa\left[\mathbf{K}_A + \frac{2}{\kappa_A h}\mathbf{C}_A + \left(\frac{2}{\kappa_A h}\right)^2 \mathbf{M}_A\right]$	$\mathbf{K}_B^* = \kappa\left[\mathbf{K}_B + \frac{2}{\kappa_B h}\mathbf{C}_B + \left(\frac{2}{\kappa_B h}\right)^2 \mathbf{M}_B\right]$

(2) Condensed operator

$$\mathbf{H} = \mathbf{L}_A[\mathbf{K}_A^*]^{-1}\mathbf{L}_A^{\mathrm{T}} + \mathbf{L}_B[\mathbf{K}_B^*]^{-1}\mathbf{L}_B^{\mathrm{T}}$$

(3) Initial conditions

$\mathbf{u}_0^A,\ \mathbf{v}_0^A,\ \mathbf{s}_0^A = \mathbf{0}$ and $\mathbf{t}_0^A = \mathbf{0}$	$\mathbf{u}_0^B,\ \mathbf{v}_0^B,\ \mathbf{s}_0^B = \mathbf{0}$ and $\mathbf{t}_0^B = \mathbf{0}$

(4) Free motion

$\mathbf{g}_n^A = \{2\bar{\mathbf{f}}^A - \mathbf{K}_A[2\mathbf{u}_n^A - (\kappa_A - 1)\mathbf{s}_n^A] + \frac{2}{\kappa_A h}\mathbf{M}_A[2\mathbf{v}_n^A - (\kappa_A - 1)\mathbf{t}_n^A]\}$	$\mathbf{g}_n^B = \{2\bar{\mathbf{f}}^B - \mathbf{K}_B[2\mathbf{u}_n^B - (\kappa_B - 1)\mathbf{s}_n^B] + \frac{2}{\kappa_B h}\mathbf{M}_B[2\mathbf{v}_n^B - (\kappa_B - 1)\mathbf{t}_n^B]\}$
$\Delta\tilde{\mathbf{u}}^A = [\mathbf{K}_A^*]^{-1}\mathbf{g}_n^A$	$\Delta\tilde{\mathbf{u}}^B = [\mathbf{K}_B^*]^{-1}\mathbf{g}_n^B$
$\Delta\tilde{\mathbf{v}}^A = \frac{2}{\kappa_A h}\Delta\tilde{\mathbf{u}}^A - \frac{1}{\kappa_A}[2\mathbf{v}_n^A - (\kappa_A - 1)\mathbf{t}_n^A]$	$\Delta\tilde{\mathbf{v}}^B = \frac{2}{\kappa_B h}\Delta\tilde{\mathbf{u}}^B - \frac{1}{\kappa_B}[2\mathbf{v}_n^B - (\kappa_B - 1)\mathbf{t}_n^B]$
$\Delta\tilde{\mathbf{s}}^A = \frac{\Delta\tilde{\mathbf{u}}^A - \mathbf{s}_n^A}{\frac{1}{2}+\alpha_A}$ and $\Delta\tilde{\mathbf{t}}^A = \frac{\Delta\tilde{\mathbf{v}}^A - \mathbf{t}_n^A}{\frac{1}{2}+\alpha_A}$	$\Delta\tilde{\mathbf{s}}^B = \frac{\Delta\tilde{\mathbf{u}}^B - \mathbf{s}_n^B}{\frac{1}{2}+\alpha_B}$ and $\Delta\tilde{\mathbf{t}}^B = \frac{\Delta\tilde{\mathbf{v}}^B - \mathbf{t}_n^B}{\frac{1}{2}+\alpha_B}$

(5) Condensed problem

$$2\bar{\boldsymbol{\lambda}} = \mathbf{H}^{-1}\{\mathbf{L}_A\Delta\tilde{\mathbf{u}}^A + 2\mathbf{L}_A\mathbf{u}_n^A + \mathbf{L}_B\Delta\tilde{\mathbf{u}}^B + 2\mathbf{L}_B\mathbf{u}_n^B\}$$

(6) Link motion

$\Delta\check{\mathbf{u}}^A = -[\mathbf{K}_A^*]^{-1}\{2\mathbf{L}_A^{\mathrm{T}}\bar{\boldsymbol{\lambda}}\}$	$\Delta\check{\mathbf{u}}^B = -[\mathbf{K}_B^*]^{-1}\{2\mathbf{L}_B^{\mathrm{T}}\bar{\boldsymbol{\lambda}}\}$
$\Delta\check{\mathbf{v}}^A = \frac{2}{\kappa_A h}\Delta\check{\mathbf{u}}^A$	$\Delta\check{\mathbf{v}}^B = \frac{2}{\kappa_B h}\Delta\check{\mathbf{u}}^B$
$\Delta\check{\mathbf{s}}^A = \frac{\Delta\check{\mathbf{u}}^A}{\frac{1}{2}+\alpha_A}$ and $\Delta\check{\mathbf{t}}^A = \frac{\Delta\check{\mathbf{v}}^A}{\frac{1}{2}+\alpha_A}$	$\Delta\check{\mathbf{s}}^B = \frac{\Delta\check{\mathbf{u}}^B}{\frac{1}{2}+\alpha_B}$ and $\Delta\check{\mathbf{t}}^B = \frac{\Delta\check{\mathbf{v}}^B}{\frac{1}{2}+\alpha_B}$

(7) Vector update:

$\mathbf{u}_{n+1}^A = \mathbf{u}_n^A + (\Delta\tilde{\mathbf{u}}^A + \Delta\check{\mathbf{u}}^A)$	$\mathbf{u}_{n+1}^B = \mathbf{u}_n^B + (\Delta\tilde{\mathbf{u}}^B + \Delta\check{\mathbf{u}}^B)$
$\mathbf{v}_{n+1}^A = \mathbf{v}_n^A + (\Delta\tilde{\mathbf{v}}^A + \Delta\check{\mathbf{v}}^A)$	$\mathbf{v}_{n+1}^B = \mathbf{v}_n^B + (\Delta\tilde{\mathbf{v}}^B + \Delta\check{\mathbf{v}}^B)$
$\mathbf{s}_{n+1}^A = \mathbf{s}_n^A + (\Delta\tilde{\mathbf{s}}^A + \Delta\check{\mathbf{s}}^A)$	$\mathbf{s}_{n+1}^B = \mathbf{s}_n^B + (\Delta\tilde{\mathbf{s}}^B + \Delta\check{\mathbf{s}}^B)$
$\mathbf{t}_{n+1}^A = \mathbf{t}_n^A + (\Delta\tilde{\mathbf{t}}^A + \Delta\check{\mathbf{t}}^A)$	$\mathbf{t}_{n+1}^B = \mathbf{t}_n^B + (\Delta\tilde{\mathbf{t}}^B + \Delta\check{\mathbf{t}}^B)$

(6) Return to (4) for next time step, or stop

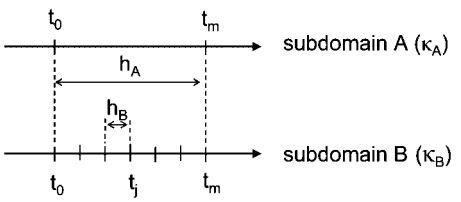

Figure 3. Two subdomains A and B integrated with individual κ parameter and time step.

DOI: 10.1002/nme

coarse time scale can be written as:

$$\left[\tfrac{1}{2}\mathbf{v}_A^{\mathrm{T}}\mathbf{M}_A\mathbf{v}_A+\tfrac{1}{2}\mathbf{u}_A^{\mathrm{T}}\mathbf{K}_A\mathbf{u}_A\right]_0^m+\sum_{j=1}^{m}\left[\tfrac{1}{2}\mathbf{v}_B^{\mathrm{T}}\mathbf{M}_B\mathbf{v}_B+\tfrac{1}{2}\mathbf{u}_B^{\mathrm{T}}\mathbf{K}_B\mathbf{u}_B\right]_{j-1}^{j}$$
$$=\bar{\bar{\Delta}}\mathbf{u}_A^{\mathrm{T}}\mathbf{L}_A^{\mathrm{T}}\bar{\bar{\boldsymbol{\lambda}}}-\tfrac{1}{2}\alpha_A(\bar{\bar{\Delta}}\mathbf{u}_A^{\mathrm{T}}\mathbf{K}_A\bar{\bar{\Delta}}\mathbf{u}_A+\bar{\bar{\Delta}}\mathbf{v}_A^{\mathrm{T}}\mathbf{M}_A\bar{\bar{\Delta}}\mathbf{v}_A)$$
$$+\sum_{j=1}^{m}\Delta\mathbf{u}_{B,j}^{\mathrm{T}}\mathbf{L}_B^{\mathrm{T}}\bar{\boldsymbol{\lambda}}_j-\tfrac{1}{2}\alpha_B\sum_{j=1}^{m}(\Delta\mathbf{u}_{B,j}^{\mathrm{T}}\mathbf{K}_B\Delta\mathbf{u}_{B,j}+\Delta\mathbf{v}_{B,j}^{\mathrm{T}}\mathbf{M}_B\Delta\mathbf{v}_{B,j}). \tag{27}$$

As in Section 4.1, the energy balance Equation (27) is the sum of the contribution of the subdomains A and B. The sum over the quantities related to the subdomain B indicates consideration of Equation (27) between two instants on the coarse time scale. An overbar on the symbol of the mean or the increment symbol defined by (8) and (9) indicates consideration of the mean or the increment of quantities between two time steps of the coarse time scale. The influence of the coupling method on the global energy balance equation can be identified as:

$$\Delta W_{\mathrm{inter}}=\bar{\bar{\Delta}}\mathbf{u}_A^{\mathrm{T}}\mathbf{L}_A^{\mathrm{T}}\bar{\bar{\boldsymbol{\lambda}}}+\sum_{j=1}^{m}\Delta\mathbf{u}_{B,j}^{\mathrm{T}}\mathbf{L}_B^{\mathrm{T}}\bar{\boldsymbol{\lambda}}_j. \tag{28}$$

The index j indicates a summation over all the contributions $\bar{\boldsymbol{\lambda}}_j$ on the fine time scale. In order to retain exact energy balance the contribution from the interface must vanish identically, i.e. $\Delta W_{\mathrm{inter}}=0$. This is obtained by setting the 'effective forces' on the fine time scale $\bar{\boldsymbol{\lambda}}_j$ equal to the representative value on the coarse scale $\bar{\bar{\boldsymbol{\lambda}}}$:

$$\bar{\boldsymbol{\lambda}}_j=\bar{\bar{\boldsymbol{\lambda}}}\quad\forall j\in[1\ldots m]. \tag{29}$$

This condition permits simplification of the interface energy expression (28) as $\Delta W_{\mathrm{inter}}=\bar{\bar{\boldsymbol{\lambda}}}^{\mathrm{T}}(\mathbf{L}_A\bar{\bar{\Delta}}\mathbf{u}^A+\sum_{j=1}^{m}\mathbf{L}_B\Delta\mathbf{u}_j^B)$. The condition $\Delta W_{\mathrm{inter}}=0$ requires $\mathbf{L}_A\bar{\bar{\Delta}}\mathbf{u}^A+\sum_{j=1}^{m}\mathbf{L}_B\Delta\mathbf{u}_j^B=\mathbf{0}$, which can be simplified as $\mathbf{L}_A\bar{\bar{\Delta}}\mathbf{u}^A+\mathbf{L}_B\bar{\bar{\Delta}}\mathbf{u}^B=\mathbf{0}$. The initial displacements are continuous at the interface, and the interface energy balance then leads to continuity of the displacement at the interfaces at each time step t_k of the coarse time scale as

$$\mathbf{L}_A\mathbf{u}_k^A+\mathbf{L}_B\mathbf{u}_k^B=\mathbf{0}\quad\forall k\in\{1,2,\ldots,n,\ldots\}. \tag{30}$$

The fully discretized equations for subdomain A over the time interval $[t_0,t_m=t_0+h_A]$ can be written as:

$$\mathbb{K}_A^*\bar{\bar{\Delta}}\mathbb{U}_A+\mathbb{L}_A\bar{\bar{\boldsymbol{\Lambda}}}=\mathbb{F}_A-\mathbb{N}_A\mathbb{U}_0^A. \tag{31}$$

Similarly, the fully discretized equations for subdomain B over the time interval $[t_{j-1},t_j=t_{j-1}+h_B],\forall j\in[1\ldots m]$ can be written as:

$$\sum_{i=1}^{j-1}\mathbb{N}_B\Delta\mathbb{U}_i^B+\mathbb{K}_B^*\Delta\mathbb{U}_j^B+\mathbb{L}_B^{\mathrm{T}}\bar{\bar{\boldsymbol{\Lambda}}}=\mathbb{F}_j^B-\mathbb{N}_B\mathbb{U}_0^B. \tag{32}$$

DOI: 10.1002/nme

Finally, Equations (30)–(32) can be represented in a general matrix form (33) as

$$\left[\begin{array}{ccccc|c|c} \mathbb{K}_B^* & & & & & & \mathbb{L}_B^{\mathrm{T}} \\ \mathbb{N}_B & \mathbb{K}_B^* & & & & & \mathbb{L}_B^{\mathrm{T}} \\ \mathbb{N}_B & \mathbb{N}_B & \mathbb{K}_B^* & & & & \mathbb{L}_B^{\mathrm{T}} \\ & \ddots & \ddots & & & & \vdots \\ \mathbb{N}_B & \mathbb{N}_B & \mathbb{N}_B & \mathbb{N}_B & \mathbb{K}_B^* & & \mathbb{L}_B^{\mathrm{T}} \\ \hline & & & & & \mathbb{K}_A^* & \mathbb{L}_A^{\mathrm{T}} \\ \hline \mathbb{L}_B & \mathbb{L}_B & \mathbb{L}_B & \mathbb{L}_B & \mathbb{L}_B & \mathbb{L}_A & \mathbf{0} \end{array}\right] \left[\begin{array}{c} \Delta\mathbb{U}_1^B \\ \Delta\mathbb{U}_2^B \\ \Delta\mathbb{U}_3^B \\ \vdots \\ \Delta\mathbb{U}_m^B \\ \hline \bar{\bar{\Delta}}\mathbb{U}_m^A \\ \hline \bar{\bar{\boldsymbol{\Lambda}}} \end{array}\right] = \left[\begin{array}{c} \mathbb{F}_1^B - \mathbb{N}_B\mathbb{U}_0^B \\ \mathbb{F}_2^B - \mathbb{N}_B\mathbb{U}_0^B \\ \mathbb{F}_3^B - \mathbb{N}_B\mathbb{U}_0^B \\ \vdots \\ \mathbb{F}_m^B - \mathbb{N}_B\mathbb{U}_0^B \\ \hline \mathbb{F}_m^A - \mathbb{N}_A\mathbb{U}_0^A \\ \hline -2\mathbb{L}_A\mathbb{U}_0^A - 2\mathbb{L}_B\mathbb{U}_0^B \end{array}\right] \tag{33}$$

Equation (33) can be solved using a bordered system approach (See Section 3). The subdomain blocks can be clubbed together and system (33) expressed as:

$$\left[\begin{array}{cc} \mathbb{K}_{A.B}^* & \mathbb{L}_{A.B}^{\mathrm{T}} \\ \mathbb{L}_{A.B} & \mathbf{0} \end{array}\right] \left[\begin{array}{c} \Delta\mathbb{U}^{A.B} \\ \bar{\boldsymbol{\Lambda}} \end{array}\right] = \left[\begin{array}{c} \mathbb{F}^{A.B} \\ -2\mathbb{L}_{A.B}\mathbb{U}_0^{A.B} \end{array}\right]. \tag{34}$$

The formalism (34) is used in the next section to present the calculation of the condensed operator in the multi-time-step case.

4.2.1. Calculation of the condensed operator in the multi-time-step case. In the presentation of the bordering approach in Section 3 it was seen that it is needed to calculate a condensed operator $\mathbb{H}$. The condensed operator $\mathbb{H} = \mathbb{L}_{A.B}\mathbb{K}_{A.B}^{-1}\mathbb{L}_{A.B}^{\mathrm{T}}$ can be obtained by first calculating the quantities $\mathbb{Y} = \mathbb{K}_{A.B}^{-1}\mathbb{L}_{A.B}^{\mathrm{T}}$ and then expressing the operator $\mathbb{H}$ as $\mathbb{H} = \mathbb{L}_{A.B}\mathbb{Y}$. The algorithm to obtain the effective matrix $\mathbf{H}$ for calculating $\bar{\bar{\lambda}}$ is given in Table VII.

4.2.2. Multi-time-scale algorithm. In this section, a general algorithm to solve Equation (33) is presented in Table VIII. The method can be generalized to s subdomains with the assumption:

$$\begin{aligned} h_1 &= m_1 h \\ h_2 &= m_2 h \\ &\cdots \qquad \text{with } \{m_1, \ldots, m_s\} \in \mathbf{N}^*. \\ &\cdots \\ h_s &= m_s h \end{aligned} \tag{35}$$

5. NUMERICAL EXAMPLE

The proposed coupling method is applied to the problem of wave propagation in a homogeneous elastic square plate with side length $4L = 0.8$, with an Young's modulus $E = 1$, a mass per unit square meter $m = 1$, and a Poisson's parameter $v = 0.3$. The plate is loaded by a force of magnitude $|\mathbf{f}| = 1$ applied at $t = 0$ and held constant at each of the four corners with an angle $\theta = 45°$. The plate

DOI: 10.1002/nme

Table VII. Calculation of the condensed operator in multi-time-step case.

(1) System matrices

$\mathbf{K}_A, \mathbf{C}_A, \mathbf{M}_A, \mathbf{L}_A, \alpha_A, h_A$	$\mathbf{K}_B, \mathbf{C}_B, \mathbf{M}_B, \mathbf{L}_B, \alpha_B, h_B$
$\kappa_A = 1+\alpha_A$	$\kappa_B = 1+\alpha_B$
$\mathbf{K}_A^* = \kappa_A \left[\mathbf{K}_A + \frac{2}{\kappa_A h_A}\mathbf{C}_A + \left(\frac{2}{\kappa_A h_A}\right)^2 \mathbf{M}_A \right]$	$\mathbf{K}_B^* = \kappa_B \left[\mathbf{K}_B + \frac{2}{\kappa_B h_B}\mathbf{C}_B + \left(\frac{2}{\kappa_B h_B}\right)^2 \mathbf{M}_B \right]$

(2) Initial conditions

$\mathbf{y}_0^A = \mathbf{0},\ \dot{\mathbf{y}}_0^A = \mathbf{0}$	$\mathbf{y}_0^B = \mathbf{0},\ \dot{\mathbf{y}}_0^B = \mathbf{0}$
(3A) Increment coarse scale	(3B) Increment fine scale—Loop $\forall j \in [1 \dots m]$
$\mathbf{G}_0^A = \left\{ -\mathbf{L}_A^{\mathrm{T}} - 2\mathbf{K}_A \mathbf{y}_0^A + \frac{4}{\kappa_A h_A}\mathbf{M}_A \dot{\mathbf{y}}_0^A \right\}$	$\mathbf{G}_{j-1}^B = \left\{ -\mathbf{L}_B^{\mathrm{T}} - 2\mathbf{K}_B \mathbf{y}_{j-1}^B + \frac{4}{\kappa_B h_B}\mathbf{M}_B \dot{\mathbf{y}}_{j-1}^B \right\}$
$\bar{\Delta}\mathbf{y}_m^A = [\mathbf{K}_A^*]^{-1}\mathbf{G}_0^A$	$\Delta\mathbf{y}_j^B = [\mathbf{K}_B^*]^{-1}\mathbf{G}_{j-1}^B$
$\bar{\Delta}\dot{\mathbf{y}}_m^A = \frac{2}{\kappa_A h_A}\bar{\Delta}\mathbf{y}_m^A - \frac{2}{\kappa_A}\dot{\mathbf{y}}_0^A$	$\Delta\dot{\mathbf{y}}_j^B = \frac{2}{\kappa_B h_B}\Delta\mathbf{y}_j^B - \frac{2}{\kappa_B}\dot{\mathbf{y}}_{j-1}^B$
(4A) Vector update	(4B) Vector update
$\mathbf{y}_m^A = \mathbf{y}_0^A + \bar{\Delta}\mathbf{y}_m^A$	$\mathbf{y}_j^B = \mathbf{y}_{j-1}^B + \Delta\mathbf{y}_j^B$
$\dot{\mathbf{y}}_m^A = \dot{\mathbf{y}}_0^A + \bar{\Delta}\dot{\mathbf{y}}_m^A$	$\dot{\mathbf{y}}_j^B = \dot{\mathbf{y}}_{j-1}^B + \Delta\dot{\mathbf{y}}_j^B$
	If $j = m$, stop loop

(5) Condensed operator

$$\mathbf{H} = \mathbf{L}_A \mathbf{y}_m^A + \mathbf{L}_B \mathbf{y}_m^B$$

is represented by four-node isoparametric quadrilateral elements under plane strain conditions. The stiffness and mass matrix are determined by a 2×2 Gaussian quadrature. The specific problem is illustrated in Figure 4. The plate is divided into eight subdomains and for symmetry reasons only a quarter of the plate is modeled. Each subdomain is integrated in time by a different numerical scheme as indicated in Figure 4(a) and with its own time scale. In this example, the balanced dissipation scheme is used. The high-frequency limit of the amplification factors used on each subdomains are indicated in Figure 4(a). The time step of the subdomain B is $h_B = mh_A$ with $m = 2$ and $h_A = 10^{-3}$. A symmetric mesh is used, and for symmetry reason the calculation is done on the quarter of the plate with the mesh shown in Figure 4(b). The highest natural frequency of the discretized system can be estimated from the free vibration frequency of a single element without supports, see e.g. [2]. It follows from this procedure that $\omega_A^e h_A = \omega_A^e h_B = 0.7686$, and algorithmic dissipation in the high-frequency regime is introduced by choosing $\lambda_\infty < 1$ as shown in Figure 5. The highest natural frequency on the finest mesh is $\omega_B^e = 122.33$.

Non-matching interfaces are used between the subdomains and thus one node of the fine mesh corresponds to two nodes of the coarse mesh neighbor. The dimension of Lagrange multipliers at the interfaces between two subdomains are equal to the dimension of the finer mesh of the interface. The continuity relations for the non-matching nodes are obtained by using the two nodes neighbor of the coarse mesh and a linear interpolation. The simulation is made on 20 time steps corresponding to the coarsest time scale B.

The displacement and velocity of the free corner node are compared with a reference solution calculated without domain decomposition with the balanced dissipation scheme with $h = 10^{-3}$ and $\lambda_\infty = 0.55$ (see Figure 6(a, b)). The results are very satisfactory both in amplitude and in phase.

DOI: 10.1002/nme

Table VIII. Coupling two subdomains with individual time scale and different numerical schemes.

(1) System matrices

$\mathbf{K}_A,\ \mathbf{C}_A,\ \mathbf{M}_A,\ \mathbf{L}_A,\ \alpha_A,\ h_A$	$\mathbf{K}_B,\ \mathbf{C}_B,\ \mathbf{M}_B,\ \mathbf{L}_B,\ \alpha_B,\ h_B$
$\kappa_A = 1+\alpha_A$	$\kappa_B = 1+\alpha_B$
$\mathbf{K}_A^* = \kappa_A\left[\mathbf{K}_A + \frac{2}{\kappa_A h_A}\mathbf{C}_A + \left(\frac{2}{\kappa_A h_A}\right)^2 \mathbf{M}_A\right]$	$\mathbf{K}_B^* = \kappa_B\left[\mathbf{K}_B + \frac{2}{\kappa_B h_B}\mathbf{C}_B + \left(\frac{2}{\kappa_B h_B}\right)^2 \mathbf{M}_B\right]$

(2) Initial conditions

$\tilde{\mathbf{u}}_0^A = \mathbf{u}_0^A,\ \tilde{\mathbf{v}}_0^A = \mathbf{u}_0^A$	$\tilde{\mathbf{u}}_0^B = \mathbf{u}_0^B,\ \tilde{\mathbf{v}}_0^B = \mathbf{v}_0^B$

(3) Free motion

(3A) Coarse scale	(3B) Fine scale—Loop $\forall j \in [1 \ldots m]$
$\bar{\Delta}\tilde{\mathbf{u}}_m^A = [\mathbf{K}_A^*]^{-1}\left\{2\bar{\mathbf{f}}^A - 2\mathbf{K}_A\tilde{\mathbf{u}}_0^A + \frac{4}{\kappa_A h_A}\mathbf{M}_A\tilde{\mathbf{v}}_0^A\right\}$	$\Delta\tilde{\mathbf{u}}_j^B = [\mathbf{K}_B^*]^{-1}\left\{2\bar{\mathbf{f}}^B - 2\mathbf{K}_B\tilde{\mathbf{u}}_{j-1}^B + \frac{4}{\kappa_B h_B}\mathbf{M}_B\tilde{\mathbf{v}}_{j-1}^B\right\}$
$\bar{\Delta}\tilde{\mathbf{v}}_m^A = \frac{2}{\kappa_A h_A}\bar{\Delta}\tilde{\mathbf{u}}_m^A - \frac{2}{\kappa_A}\tilde{\mathbf{v}}_0^A$	$\Delta\tilde{\mathbf{v}}_j^B = \frac{2}{\kappa_B h_B}\Delta\tilde{\mathbf{u}}_j^B - \frac{2}{\kappa_B}\tilde{\mathbf{v}}_{j-1}^B$
$\tilde{\mathbf{u}}_m^A = \tilde{\mathbf{u}}_0^A + \bar{\Delta}\tilde{\mathbf{u}}_m^A$ and $\tilde{\mathbf{v}}_m^A = \tilde{\mathbf{v}}_0^A + \bar{\Delta}\tilde{\mathbf{v}}_m^A$	$\tilde{\mathbf{u}}_j^B = \tilde{\mathbf{u}}_{j-1}^B + \Delta\tilde{\mathbf{u}}_j^B$ and $\tilde{\mathbf{v}}_j^B = \tilde{\mathbf{v}}_{j-1}^B + \Delta\tilde{\mathbf{v}}_j^B$
	If $j = m$, stop loop

(4) Condensed problem

$$2\bar{\bar{\boldsymbol{\lambda}}} = \mathbf{H}^{-1}\{\mathbf{L}_A\bar{\Delta}\tilde{\mathbf{u}}_m^A + 2\mathbf{L}_A\mathbf{u}_0^A + \mathbf{L}_B\bar{\Delta}\tilde{\mathbf{u}}_m^B + 2\mathbf{L}_B\mathbf{u}_0^B\}$$

(5) Link motion

(5A) Coarse scale	(5B) Fine scale—Loop $\forall j \in [1 \ldots m]$
$\check{\mathbf{u}}_0^A = \mathbf{0}$ and $\check{\mathbf{v}}_0^A = \mathbf{0}$	$\check{\mathbf{u}}_0^B = \mathbf{0}$ and $\check{\mathbf{v}}_0^B = \mathbf{0}$
$\bar{\Delta}\check{\mathbf{u}}_m^A = [\mathbf{K}_A^*]^{-1}\left\{-2\mathbf{L}_A^{\mathrm{T}}\bar{\bar{\boldsymbol{\lambda}}} - 2\mathbf{K}_A\check{\mathbf{u}}_0^A + \frac{4}{\kappa_A h_A}\mathbf{M}_A\check{\mathbf{v}}_0^A\right\}$	$\Delta\check{\mathbf{u}}_j^B = [\mathbf{K}_B^*]^{-1}\left\{-2\mathbf{L}_B^{\mathrm{T}}\bar{\bar{\boldsymbol{\lambda}}} - 2\mathbf{K}_B\check{\mathbf{u}}_{j-1}^B + \frac{4}{\kappa_B h_B}\mathbf{M}_B\check{\mathbf{v}}_{j-1}^B\right\}$
$\bar{\Delta}\check{\mathbf{v}}_m^A = \frac{2}{\kappa_A h_A}\bar{\Delta}\check{\mathbf{u}}_m^A - \frac{2}{\kappa_A}\check{\mathbf{v}}_0^A$	$\Delta\check{\mathbf{v}}_j^B = \frac{2}{\kappa_B h_B}\Delta\check{\mathbf{u}}_j^B - \frac{2}{\kappa_B}\check{\mathbf{v}}_{j-1}^B$
$\check{\mathbf{u}}_m^A = \check{\mathbf{u}}_0^A + \bar{\Delta}\check{\mathbf{u}}_m^A$ and $\check{\mathbf{v}}_m^A = \check{\mathbf{v}}_0^A + \bar{\Delta}\check{\mathbf{v}}_m^A$	$\check{\mathbf{u}}_j^B = \check{\mathbf{u}}_{j-1}^B + \Delta\check{\mathbf{u}}_j^B$ and $\check{\mathbf{v}}_j^B = \check{\mathbf{v}}_{j-1}^B + \Delta\check{\mathbf{v}}_j^B$
	If $j = m$, stop loop

(6) Vector update

(6A) Coarse scale	(6B) Fine scale—Loop $\forall j \in [1 \ldots m]$
$\mathbf{u}_m^A = \tilde{\mathbf{u}}_m^A + \check{\mathbf{u}}_m^A$ and $\mathbf{v}_m^A = \tilde{\mathbf{v}}_m^A + \check{\mathbf{v}}_m^A$	$\mathbf{u}_j^B = \tilde{\mathbf{u}}_j^B + \check{\mathbf{u}}_j^B$ and $\mathbf{v}_j^B = \tilde{\mathbf{v}}_j^B + \check{\mathbf{v}}_j^B$
	If $j = m$, stop loop

(7) Return to (3) for next time step, or stop

Figure 7 shows the energy balance of the method with domain decomposition for the case $m = 2$. Thus, it is verified that the work of the interface forces is identically zero.

6. CONCLUSIONS

A multi-time-step integration method has been proposed for coupling subdomains integrated in time using different time steps and/or different state-space time integration schemes. In this manner,

DOI: 10.1002/nme

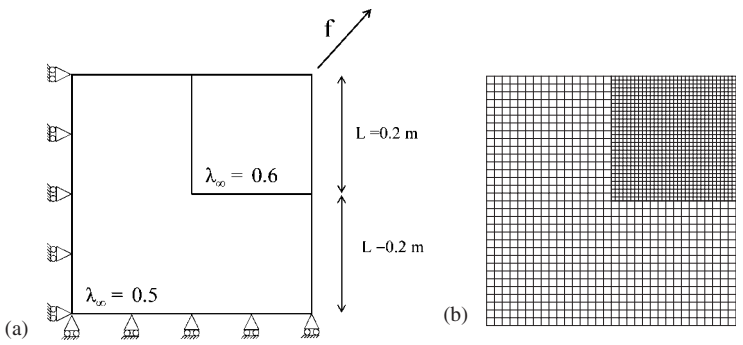

Figure 4. Plate loaded by a force at the four corner: (a) plate divided into two subdomains and (b) FE model.

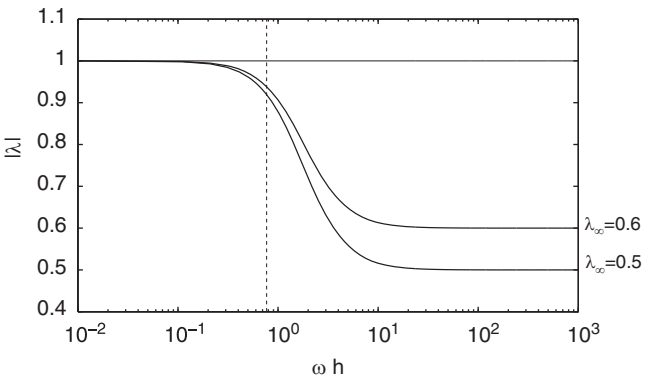

Figure 5. Spectral properties.

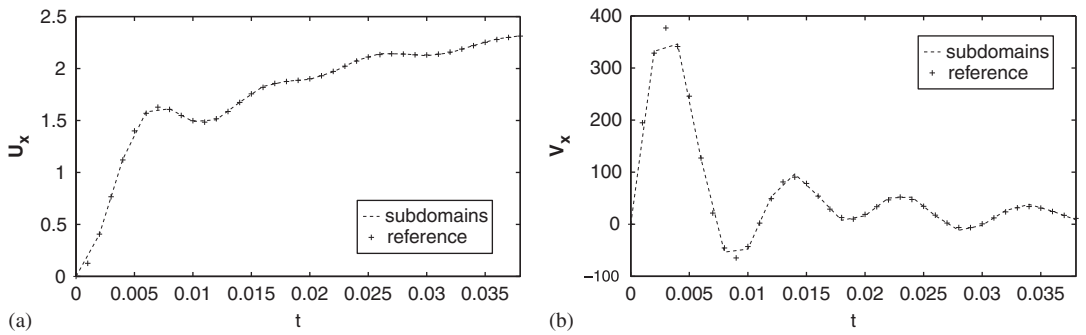

Figure 6. Kinematics of the free corner node: (a) displacement and (b) velocity.

the user may control the algorithmic damping introduced in each subdomain by choosing locally the most suitable algorithmic parameters and time steps. The formulations of both state-space time integration schemes, the balanced dissipation algorithm and the high-frequency algorithm, have

DOI: 10.1002/nme

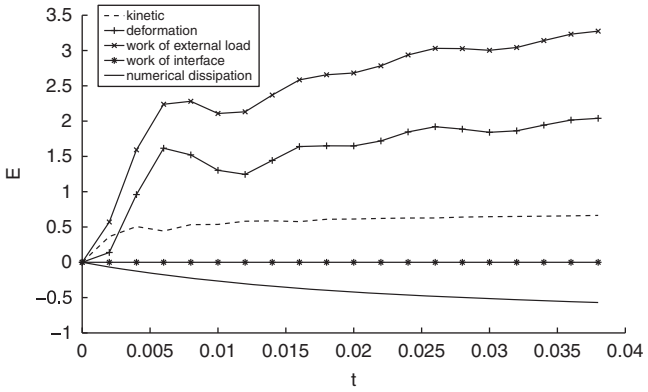

Figure 7. Energy balance.

been extended to include constraints via Lagrange multipliers. The Lagrange multipliers represent the time-averaged constraint forces and appear as additional unknowns in an augmented state-space vector. This allows the coupling method to be written in a Schur dual formalism where the link between the subdomains is ensured through Lagrange multipliers. The energy balance equation has been used to analyze the global stability of the coupling which is achieved by imposing continuous displacements at the interfaces between the subdomains. The change in energy at the interface is identically zero by construction, and thus coupling does not affect the global stability of the problem. The computations on each subdomain are independent, except for the computation of the interface forces, which is a smaller problem than the global one. Hence, the proposed method is well suited for parallel implementation.

REFERENCES

1. Newmark NM. A method of computation for structural dynamics. *Journal of the Engineering Mechanics Division* (ASCE) 1959; **85**:67–94.
2. Hughes TJR. *The Finite Element Method*: *Linear Static and Dynamic Finite Element Analysis*. Prentice-Hall: Englewood Cliffs, NJ, 1987.
3. Hilber HM, Hughes TJR, Taylor RL. Improved numerical dissipation for time integration algorithms in structural dynamics. *Earthquake Engineering and Structural Dynamics* 1977; **5**:283–292.
4. Wood WL, Bossak M, Zienkiewicz OC. An α modification of Newmark's method. *International Journal for Numerical Methods in Engineering* 1980; **15**:1562–1566.
5. Chung J, Hulbert GM. Time integration algorithm for structural dynamics with improved numerical dissipation: the generalized-α method. *Journal of Applied Mechanics* 1993; **60**:371–375.
6. Krenk S, Høgsberg JR. Properties of time integration with first order filter damping. *International Journal for Numerical Methods in Engineering* 2005; **64**:547–566.
7. Krenk S. Energy conservation in Newmark based time integration algorithms. *Computer Methods in Applied Mechanics and Engineering* 2006; **195**:6110–6124.
8. Simo JC, Tarnow N. The discrete energy-momentum method. Conserving algorithms for nonlinear elastodynamics. *Zeitschrift für Angewandte Mathematik und Physik* (*ZAMP*) 1992; **43**:757–792.
9. Armero F, Romero I. On the formulation of high-frequency dissipative time-stepping algorithms for nonlinear dynamics. Part I: low-order methods for two model problems and nonlinear elastodynamics. *Computer Methods in Applied Mechanics and Engineering* 2001; **190**:2603–2649.
10. Betsch P, Steinmann P. Conservation properties of a time FE method. Part III: mechanical systems with holonomic constraints. *International Journal for Numerical Methods in Engineering* 2002; **53**:2271–2304.

DOI: 10.1002/nme

11. Krenk S. Extended state-space time integration with high-frequency energy dissipation. *International Journal for Numerical Methods in Engineering* 2008; **73**:1767–1787.
12. Krenk S. *Non-linear Modeling and Analysis of Solids and Structures*. Cambridge University Press: Cambridge, U.K., 2009.
13. Krenk S. The role of geometric stiffness in momentum and energy conserving time integration. *International Journal for Numerical Methods in Engineering* 2007; **71**:631–651.
14. Krenk S. State-space time integration with energy control and fourth-order accuracy for linear dynamic systems. *International Journal for Numerical Methods in Engineering* 2006; **65**:595–619.
15. Liu WK, Belytschko T. Mixed-time implicit-explicit finite elements for transient analysis. *Computers and Structures* 1982; **15**:445–450.
16. Belytschko T, Mullen R. Stability of explicit-implicit mesh partitions in time integration. *International Journal for Numerical Methods in Engineering* 1978; **12**:1575–1586.
17. Hughes TJR, Liu WK. Implicit-explicit finite elements in transient analysis: stability theory. *Journal of Applied Mechanics* 1978; **45**:371–374.
18. Daniel WJT. The subcycled Newmark algorithm. *Computational Mechanics* 1997; **20**:272–281.
19. Belytschko T. Mixed methods for time integration. *Computer Methods in Applied Mechanics and Engineering* 1979; **17–18**:259–275.
20. Park KC. Partitioned transient analysis procedures for coupled-field problems: stability analysis. *Journal of Applied Mechanics* 1980; **47**:370–376.
21. Smolinski P, Belytschko T, Neal M. Multi-time-step integration using nodal partitioning. *International Journal for Numerical Methods in Engineering* 1988; **26**:349–359.
22. Farhat C, Roux F-X. A method of finite element tearing and interconnecting and its parallel solution algorithm. *International Journal for Numerical Methods in Engineering* 1991; **32**:1205–1227.
23. Farhat C, Crivelli L, Roux F-X. A transient FETI methodology for large-scale parallel implicit computations in structural mechanics. *International Journal for Numerical Methods in Engineering* 1994; **37**:1945–1975.
24. Farhat C, Crivelli L, Géradin M. Implicit time integration of a class of constrained hybrid formulations. Part I: spectral stability theory. *Computer Methods in Applied Mechanics and Engineering* 1995; **125**:71–107.
25. Gravouil A, Combescure A. Multi-time-step explicit-implicit method for non-linear structural dynamics. *International Journal for Numerical Methods in Engineering* 2001; **50**:199–225.
26. Combescure A, Gravouil A. A numerical scheme to couple subdomains with different time-steps for predominantly linear transient analysis. *Computer Methods in Applied Mechanics and Engineering* 2002; **191**:1129–1157.
27. Faucher V, Combescure A. Local modal reduction in explicit dynamics with domain decomposition. Part 1: extension to subdomains undergoing finite rigid rotations. *International Journal for Numerical Methods in Engineering* 2004; **60**:2531–2560.
28. Combescure A, Gravouil A, Herry B. An algorithm to solve transient structural non-linear problems for non-matching time-space domains. *Computers and Structures* 2003; **81**:1211–1222.
29. Prakash A, Hjelmstad KD. A FETI-based multi-time-step coupling method for Newmark schemes in structural dynamics. *International Journal for Numerical Methods in Engineering* 2004; **61**:2183–2204.
30. Govaerts W. Stable solvers and block elimination for bordered systems. *SIAM Journal on Matrix Analysis and Applications* 1991; **12**:469–483.

DOI: 10.1002/nme